Check for updates

A multifunctional composite Fe₃O₄/MOF/L-cysteine for removal, magnetic solid phase extraction and fluorescence sensing of Cd(II)†

Lu Fan,‡[a] Min Deng,‡[a] Caixue Lin,[a] Chen Xu,[a] Yana Liu,[a] Zhennan Shi,[a] Yingxi Wang,[a] Zushun Xu, [ID][a] Ling Li [ID]*[a] and Man He*[b]

Fe₃O₄/MOF (metal organic framework)/L-cysteine was synthesized and applied for the removal of Cd(II) from wastewater. The adsorption kinetics and isotherms were investigated, and the results indicated that the adsorption obeyed the pseudo-second-order kinetic model and Langmuir isotherm. The maximum adsorption capacity was calculated to be 248.24 mg g^{-1}. Fe₃O₄/MOF/L-cysteine was further applied to determine trace amounts of Cd(II) in real water samples using ICP-AES (inductively coupled plasma-atomic emission spectroscopy) based on magnetic solid-phase extraction (MSPE). The determination limit was 10.6 ng mL^{-1}. Additionally, Fe₃O₄/MOF/L-cysteine can also be used as a fluorescent sensor for "turn-off" detection of Cd(II), and the detection limit was 0.94 ng mL^{-1}.

1. Introduction

Cadmium ions are heavy metal ions that are highly toxic to human beings,[1–3] and as they can be accumulated through the food chain, they can cause great harm to people by causing kidney failure, anemia, cardiovascular diseases, growth impairment and loss of taste and smell.[4] Therefore, it is of great significance to remove Cd(II) from water solutions and develop an effective method of determination for trace amounts of Cd(II).

Many methods to remove cadmium ions have been reported, such as adsorption, precipitation, ion exchange, and membrane filtration. Adsorption is regarded as one of the most competitive methods because of its convenient operation and excellent treatment effect. In the process of adsorption, the adsorbent must have excellent stability and adsorption capacity. Furthermore, on the basis of the adsorbent, solid-phase extraction (SPE)[5] and magnetic solid phase extraction (MSPE)[6] can be set up to determine trace amounts of Cd(II).

SPE is widely used as a sample pretreatment method because of its high recovery rate, short extraction time, high preconcentration factor and easy automation.[7] However, it may be difficult to completely separate and remove the adsorbent from the aqueous

solution and may cause additional environmental problems. To overcome these disadvantages, magnetic solid phase extraction (MSPE) using magnetic nanoparticles has been developed, and the phase separation of the solid magnetic absorbent from the liquid sample can be done directly using an external magnet without the need for additional filtration or centrifugation procedures, which makes separation faster and easier. Generally, mostly magnetic adsorbents are composites of Fe₃O₄.

As the adsorbent plays an important role in Cd(II) removal and analysis, the design of the adsorbent is very important. Zhang synthesized Fe₃O₄/PANI/MnO₂ hybrids materials as advanced adsorbents for removal of heavy metal ions.[8] Lin prepared Fe₃O₄@SH nanoparticles for Cd(II) removal.[9] Chen prepared Fe₃O₄@SiO₂–NH-HCGs for removal of Cu(II), Hg(II), Pb(II) and Cd(II).[10] However, these materials had limited functional modification, specific surface area and adsorption capacity. Therefore, the design of an efficient magnetic composite is attracting researchers' interests.

Metal organic frameworks (MOFs), also known as coordination polymers or coordination networks, are unique crystalline materials formed by connecting metal centers and organic ligands into infinite arrays through dative bonds. MOFs have attracted much attention for their high porosity, large specific surface area, and easy for functional modification. The structure formed by Cu(II) and 5-aminoisophthalic acid (AIPA) is relatively stable, with relatively large specific surface area and suitable pore volume, which make it suitable for the adsorption of toxic heavy metal ions. Cu(II) was selected as the central ion, and 5-aminoisophthalic acid (AIPA) was chosen as the ligand. The coordination between the Cu(II) and the oxygen atoms of the ligand leads to the formation of the basic unit, which results in the porous structure of MOFs. On the basis of the porous

[a] Hubei Collaborative Innovation Center for Advanced Organic Chemical Materials, Ministry-of-Education Key Laboratory for the Synthesis and Application of Organic Function Molecules, Hubei University, 430062, People's Republic of China. E-mail: lingli@hubu.edu.cn; Fax: +86-27-88663043; Tel: +86-27-88662747

[b] Department of Chemistry, Wuhan University, Wuhan City, Hubei Province 430074, People's Republic of China. E-mail: heman@whu.edu.cn; Fax: +86-27-68754685; Tel: +86-27-68756759

† Electronic supplementary information (ESI) available. See DOI: 10.1039/c8ra00070k

‡ These authors contributed equally to this work.
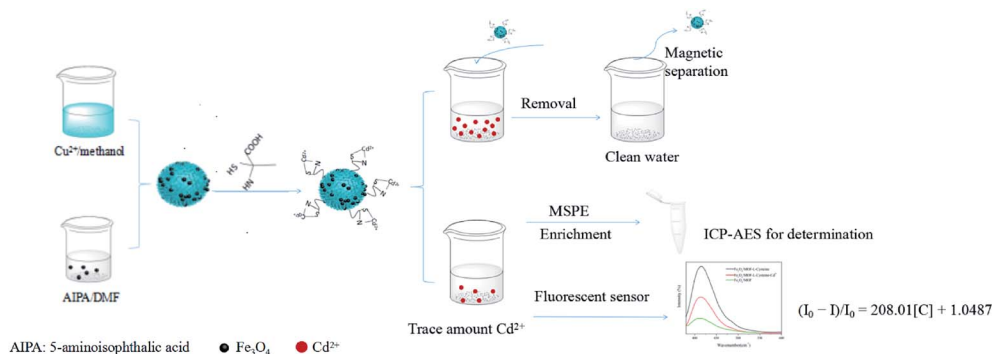
Scheme 1 Schematic illustration of the synthesis of Fe_3O_4/MOF/L-cysteine for Cd(II) removal.

structure, the addition of nano-Fe_3O_4 particles can form a magnetic composite that can potentially be used for MSPE. Safari prepared two kinds of Fe_3O_4/MOF and applied them to the preconcentration of the ions Co(II), Cu(II), Pb(II), Cd(II), Ni(II), Cr(III), and Mn(II) from aqueous solutions.[11] Wang reported SH-Fe_3O_4/Cu_3(BTC)$_2$ composites for the extraction and determination of trace amounts of lead in food samples.[12] On the other hand, MOFs are widely reported as fluorescent sensors to determine trace amounts of metal ions. Xing synthesized a Zn-MOF using a multiwalled divider installation strategy for sensing Co(II).[13] Li synthesized a luminescent mesoporous Zn_2TiO_4:Eu^{3+} material for sensing heavy metal ions.[14] Wu prepared a porous Zn-MOF for fluorescence sensing of Cu(II).[15] In recent years, MOFs for the fluorescence sensing of Cd(II) have seldom been reported. Therefore, in this study, a combination of a MOF and Fe_3O_4 nanoparticles was used to form a magnetic composite, which was further modified by functional groups to sense metal ions. A kind of multifunctional material for the removal, magnetic solid phase extraction and fluorescence sensing of Cd(II) was obtained.

In this work, L-cysteine is used, which is a kind of natural amino acid with three types of functional group (–SH, –NH_2 and –COOH) that could coordinate with Cd(II). Hence, Fe_3O_4/MOF was prepared, and further modified using L-cysteine to form Fe_3O_4/MOF/L-cysteine, as shown in Scheme 1. Fe_3O_4/MOF/L-cysteine was used as an MSPE adsorbent to remove Cd(II). A method of MSPE coupled with inductively coupled plasma-atomic emission spectroscopy (ICP-AES) for the analysis of Cd(II) was introduced. The conditions of adsorption–desorption were investigated. Furthermore, the kinetics for the adsorption model and the adsorption isotherms were investigated under optimal conditions, and the maximum adsorption capacity was calculated. In addition, Fe_3O_4/MOF/L-cysteine was investigated for detecting trace amounts of Cd(II). The analysis of real samples was further investigated. The material's reusability and the limit of detection (LOD) were evaluated.

2. Materials and methods

2.1. Chemicals and reagents

All chemicals used were at least of analytical grade. Hexahydrate ferric chloride, anhydrous sodium acetate, copper nitrate trihydrate, sodium borohydride, sodium dihydrogen phosphate dihydrate, dodecahydrate disodium hydrogen phosphate, Tris (tris(hydroxymethyl) aminomethane)–HCl buffer, cadmium chloride, zinc nitrate, ferric chloride, chromic nitrate, lead nitrate, mercury nitrate, glutaraldehyde, ethylene glycol, anhydrous methanol, anhydrous ethanol and DMF (dimethylformamide) were obtained from Sinopharm Chemical Reagent Co., Ltd. (Shanghai, China). 5-Aminoisophthalic acid (AIPA) and L-cysteine were obtained from Aladdin (Shanghai, China). Ultrapure water (18.2 MU cm) was obtained from a WaterPro Water Purification System (Labconco Corporation, Kansas City, MO, USA). Ultrapure water was used in all experiments.

The stock solution of Cd(II) (1000 ppm) was prepared by dissolving cadmium chloride in ultrapure water, and this was diluted to different concentrations for use. The Cd(II) concentrations were determined using ICP-AES spectroscopy. A calibration curve was obtained from the spectra of the standard solutions and was used to determine the residual concentrations of Cd(II) in solution. Phosphate buffer solutions (from pH 7.0 to pH 9.0) were prepared with different amounts of NaH_2PO_4 and Na_2HPO_4. Tris–HCl buffer solutions (from pH 3.0 to pH 6.0) were prepared with different volumes of Tris solution and HCl solution.

2.2. Instruments

Powder X-ray diffractometry (XRD) patterns were obtained using a D8 Advance X-ray diffractometer (Bruker Company, Germany). Fourier Transform Infra-Red (FT-IR) spectra were obtained using a Spectrum One FT-IR spectrophotometer (Perkin-Elmer, USA) at room temperature. Scanning electron microscope (SEM) images were obtained using a JSM6510LV scanning electron microscope (JEOL, Japan), and elemental analysis was performed using Energy Dispersive X-ray Spectroscopy (EDS) (JEOL, Japan). The thermal stability of the composites was investigated using a Thermo Gravimetric Analyzer (TGA) (TGA2, METTLER TOLEDO). N_2 adsorption–desorption analysis was performed on an Accelerated Surface Area and Porosimetry System ASAP2020 (Micromeritics, USA). The surface area was estimated using the BET equation, and the pore size distribution was determined using the BJH model. Heavy metal ion

concentrations were determined using inductively coupled plasma atomic emission spectroscopy (ICP-AES) (Optima 8000, Perkin-Elmer, USA).

2.3. Synthesis of Fe_3O_4 nanoparticles

The magnetic nanoparticles were prepared according to a literature procedure with some modifications.[16] Briefly, 1.73 g $FeCl_3 \cdot 6H_2O$ (6.40 mmol) was dissolved in ethylene glycol (35 mL), then 2.31 g NaAc (28.15 mmol) was added with magnetic stirring. After stirring for 30 minutes, the mixture was transferred to a 50 mL Teflon autoclave and heated at 200 °C for 8 h before cooling to room temperature. The black products were washed with ethanol and water several times, dried at 80 °C for 6 hours, and the Fe_3O_4 nanoparticles were obtained.

2.4. Synthesis of Fe_3O_4/MOF

The Fe_3O_4/MOF crystals were prepared according to literature procedures with some modifications.[17,18] Typically, 0.10 g nano-Fe_3O_4 (0.45 mmol) and 0.4529 g (2.50 mmol) AIPA were ultrasonically dispersed in 20 mL DMF for 30 min, and marked solution A. 1.08 g $Cu(NO_3)_2$ (4.50 mmol) was dispersed in 15 mL anhydrous methanol for 30 min, and marked solution B. Solution A and solution B were homogeneously mixed and then transferred to a Teflon autoclave for reaction at 120 °C for 12 h. The resulting crystals were washed with ethanol and water several times, respectively. The Fe_3O_4/MOF composites were obtained using magnetic separation and dried for 6 hours at 80 °C. According to the reported literature,[18] the formula of the MOF is $[Cu(C_8H_6NO_4)_2]_n$, and the structure is shown in Scheme 2.

2.5. Synthesis of Fe_3O_4/MOF/L-cysteine

Fe_3O_4/MOF/L-cysteine was prepared according to a literature procedure with some modifications.[19] Typically, 1.00 g of the Fe_3O_4/MOF composite was added to 100 mL of phosphate buffer (pH = 8.0) containing 5% glutaraldehyde and transferred to a 250 mL flask, then mechanically stirred at room temperature for 2 hours. After the product was separated and washed with ultrapure water three times, 0.30 g L-cysteine and 100 mL

Scheme 2 The structure of the MOF.

phosphate buffer (pH = 8.0) were added to the flask, and mechanically stirred for 2 h. 0.50 g $NaBH_4$ was then added slowly and mechanical stirring was maintained for 6 hours. The product was separated and treated with ethanol and ultrapure water several times, then vacuum dried at 60 °C for 8 hours. Fe_3O_4/MOF/L-cysteine was obtained.

2.6. Adsorption and desorption experiments

Before adsorption, the absorbent (50.00 mg) was added to a 100 mL sample solution with 1.000 ppm of Cd(II), Zn(II), Fe(III), Cu(II), Hg(II), and Pb(II), respectively. The mixture was shaken well for a fixed time from 2 to 20 min at room temperature. After reaching adsorption equilibrium, the absorbent was separated from the mixed solution using an external magnet. The concentration of residual heavy metal ions was determined using ICP-AES spectroscopy.

The feasibility of regenerating the exhausted absorbent was evaluated using 1.0 mol L^{-1} HCl. The eluent solution was added to the used absorbent and ultrasonicated for 20 min.

## 2.7. Determination of the maximum adsorption capacity

The experiment to determine the maximum adsorption capacity was as follows: first, 0.05 g Fe_3O_4/MOF/L-cysteine was immersed in a solution with 10 ppm Cd(II). After obtaining adsorption equilibrium, the equilibrium adsorption capacity was calculated, and the Fe_3O_4/MOF/L-cysteine was dried and immersed in another solution with 20 ppm Cd(II) until adsorption equilibrium was again obtained. This was repeated until no Cd(II) could be adsorbed by the Fe_3O_4/MOF/L-cysteine. The sum of each equilibrium adsorption capacity was the maximum adsorption capacity.

2.8. MSPE procedures

50.00 mg Fe_3O_4/MOF/L-cysteine was added to a 100 mL sample solution with 0.100 ppm of Cd(II) in a conical flask. The mixture was shaken at 200 rpm for 20 min before the Fe_3O_4/MOF/L-cysteine was magnetically separated from the sample solution. 1.0 mL 1 mol L^{-1} HCl was added to the used Fe_3O_4/MOF/L-cysteine and the mixture was ultrasonicated for 20 min. 3 mL desorption solution was injected into the ICP-AES system for analysis. After being washed several times with absolute ethanol and water using a centrifuge for 5 min, the extraction experiment was carried out at room temperature. The Fe_3O_4/MOF/L-cysteine was reused for the next magnetic solid phase extraction.

2.9. Fluorescence sensing experiment

3.00 mg Fe_3O_4/MOF/L-cysteine and 3.00 mg Fe_3O_4/MOF were added into separate DMF solutions (10 mL), ultrasonicated for 20 min, and the fluorescence intensities of Fe_3O_4/MOF and Fe_3O_4/MOF/L-cysteine were determined using a fluorescence spectrometer (Perkin-Elmer LS55, USA), with an excitation wavelength of 330 nm. DMF solutions of different concentrations of Cd(II) (0.000 ppm, 0.002 ppm, 0.005 ppm, 0.020 ppm, 0.050 ppm, 0.100 ppm) were added to each solution, and the
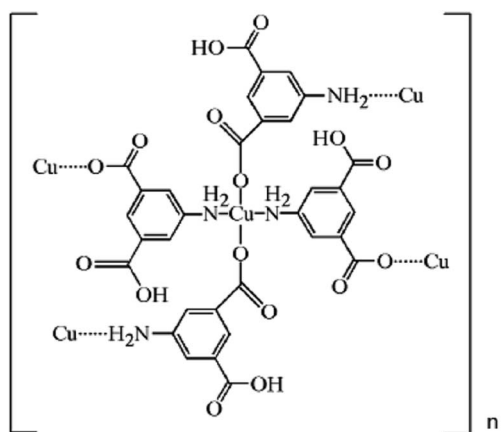
fluorescence intensities of $Fe_3O_4/MOF/Cd^{2+}$ and $Fe_3O_4/MOF/L$-cysteine/Cd^{2+} were determined after the mixed solutions were ultrasonicated for 5 min at room temperature.

2.10. Real sample analysis

In order to evaluate the accuracy of the procedure, an equal mass of $Fe_3O_4/MOF/L$-cysteine (50.00 mg) was added into 100 mL tap water and lake water, respectively. After the reaction, the adsorbent and the solution were separated using a magnet, then the adsorbent was eluted with an eluent. The cadmium ions in the eluate were measured using ICP-AES.

3. Results and discussion

3.1. Characterization of Fe_3O_4/MOF and $Fe_3O_4/MOF/L$-cysteine

The XRD patterns of Fe_3O_4, L-cysteine, Fe_3O_4/MOF, $Fe_3O_4/MOF/$L-cysteine and $Fe_3O_4/MOF/L$-cysteine after adsorption are shown in Fig. 1. Six discernible diffraction peaks of Fe_3O_4 are at 30.2°, 35.6°, 43.1°, 53.5°, 57.0° and 62.6°, which are indexed as (220), (311), (400), (422), (511), and (440), respectively. The results correspond well to the standard characteristic peaks of Fe_3O_4 (JCPDS 75-1609).

Compared with the diffraction peaks of Fe_3O_4, the peaks of Fe_3O_4/MOF and $Fe_3O_4/MOF/L$-cysteine shift a little, which is probably caused by the formation of composite materials between the Fe_3O_4, MOF and L-cysteine, which has an effect on the crystal's structure. The diffraction peaks of L-cysteine are observed at 10.2°, 14.9°, 20.8° and 42.2°, and are observed in $Fe_3O_4/MOF/L$-cysteine, indicating that $Fe_3O_4/MOF/L$-cysteine is successfully synthesised and that the crystalline forms of $Fe_3O_4/$ MOF and L-cysteine don't change when the $Fe_3O_4/MOF/L$-cysteine composites are prepared. Comparing Fig. 1(d) with Fig. 1(e), the diffraction peaks of $Fe_3O_4/MOF/L$-cysteine after

adsorption don't obviously change, so we can make a conclusion that $Fe_3O_4/MOF/L$-cysteine has good stability.

In addition, Fe_3O_4, L-cysteine, Fe_3O_4/MOF, $Fe_3O_4/MOF/L$-cysteine and $Fe_3O_4/MOF/L$-cysteine after adsorption were further investigated using FT-IR spectroscopy, and the spectra are shown in Fig. 2. Although the spectra of Fe_3O_4/MOF and $Fe_3O_4/MOF/L$-cysteine are similar, there are obvious changes in the spectrum of $Fe_3O_4/MOF/L$-cysteine. The characteristic lattice vibration of Fe–O at about 580 cm^{-1} is obvious, indicating that the sample contains Fe_3O_4 in the Fe_3O_4/MOF and $Fe_3O_4/MOF/L$-cysteine spectra. The strong stretching-vibration bands in the range of 3000–3500 cm^{-1} belong to –OH and –NH_2. The peak at 1734 cm^{-1} belongs to the stretching-vibrations of C=O. Compared to the Fe_3O_4/MOF spectrum, the peaks at 2582 cm^{-1} and 545 cm^{-1} in the L-cysteine and $Fe_3O_4/MOF/L$-cysteine spectra belong to the stretching-vibrations and bending-vibrations of S–H, and the peaks of S–H are weakened because of the small amounts of L-cysteine, which indicates the successful immobilization of L-cysteine on Fe_3O_4/MOF. As for the FT-IR spectrum of $Fe_3O_4/MOF/L$-cysteine after adsorption, the peak at 1734 cm^{-1} of the C=O group and the peaks of 3000–3200 cm^{-1} of –NH_2 stay nearly unchanged. However, the peaks of 2582 cm^{-1} and 545 cm^{-1}, which are attributed to the stretching-vibrations and bending-vibrations of S–H, disappear. It can be concluded that the adsorption force is the coordination between the S–H group and Cd(II). Therefore, there is chemical adsorption.

The SEM images of Fe_3O_4/MOF, $Fe_3O_4/MOF/L$-cysteine, and $Fe_3O_4/MOF/L$-cysteine after adsorption, and EDS are shown in Fig. 3. It can be seen that the MOFs are flower-like clusters, and the particles on the MOF surface are Fe_3O_4 nanoparticles, which demonstrates that Fe_3O_4 particles are embedded in the MOF loose surface, as shown in Fig. 3(a and b). In comparison, the surface of $Fe_3O_4/MOF/L$-cysteine (Fig. 3(c and d)) is significantly different from that of Fe_3O_4/MOF. The $Fe_3O_4/MOF/L$-cysteine
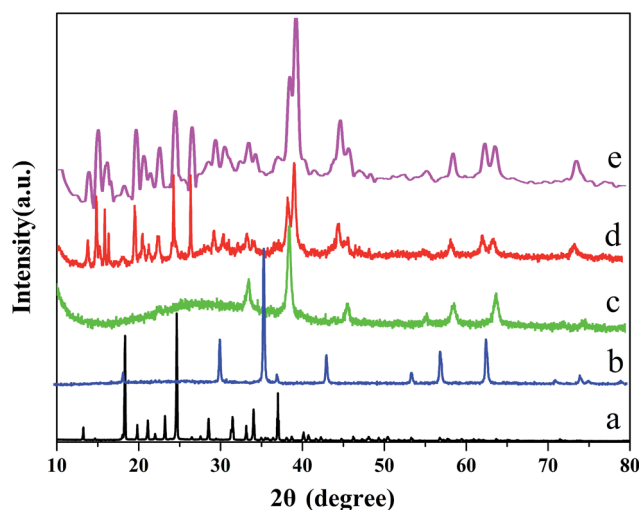
Fig. 1 X-ray diffraction patterns of (a) L-cysteine, (b) Fe_3O_4, (c) $Fe_3O_4/$MOF, (d) $Fe_3O_4/MOF/L$-cysteine, and (e) $Fe_3O_4/MOF/L$-cysteine after adsorption.
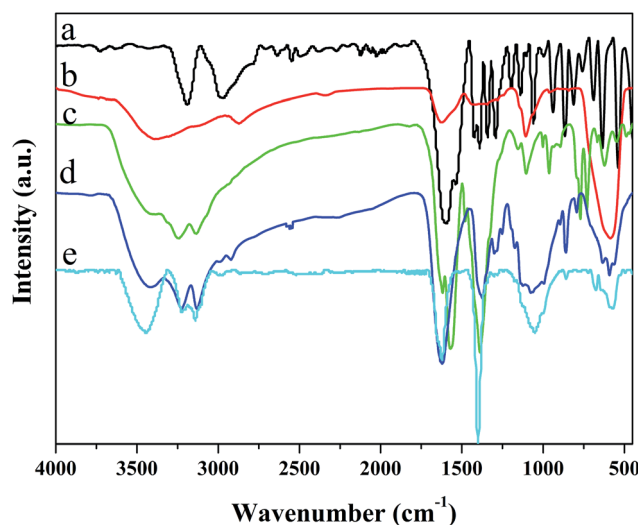
Fig. 2 FT-IR spectra of (a) L-cysteine, (b) Fe_3O_4, (c) Fe_3O_4/MOF, (d) $Fe_3O_4/MOF/L$-cysteine, and (e) $Fe_3O_4/MOF/L$-cysteine after adsorption.
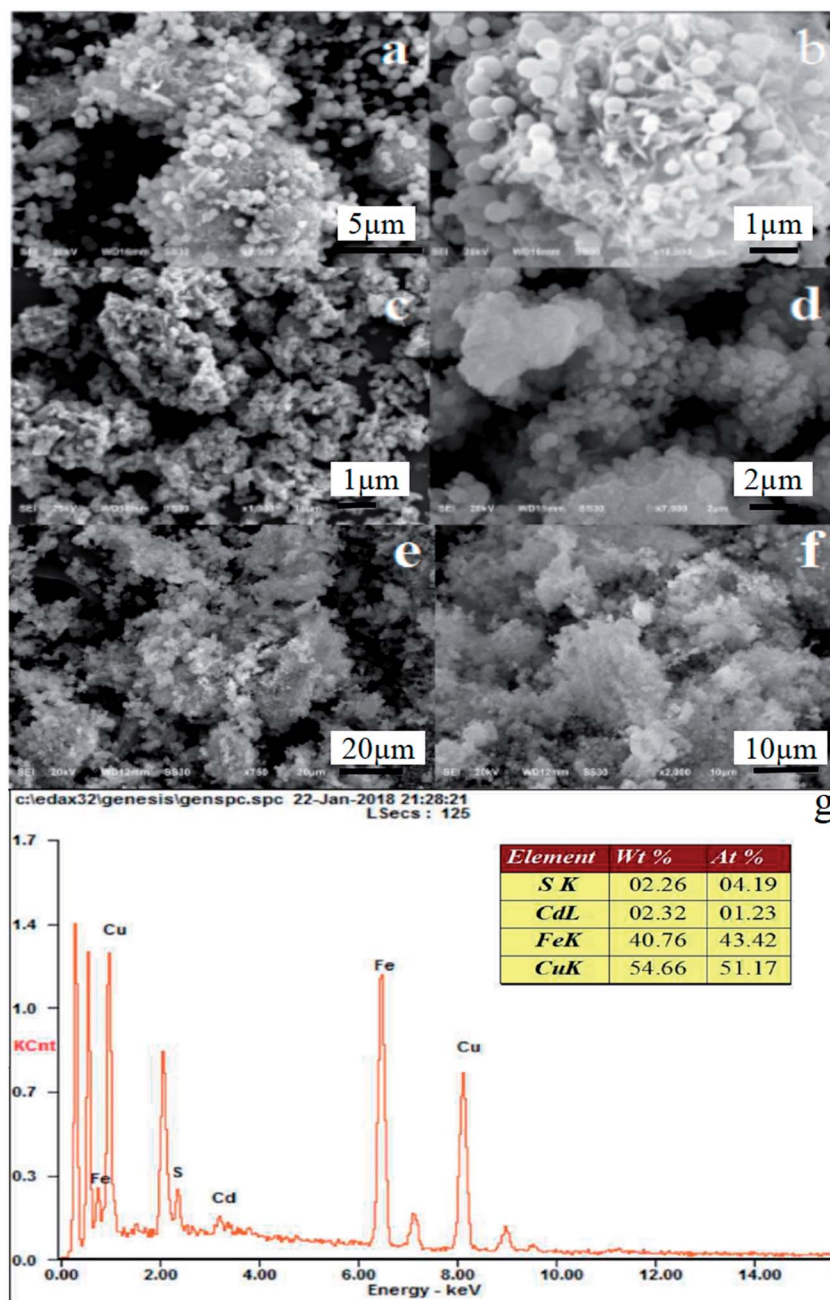
Fig. 3 SEM images of Fe_3O_4/MOF (a and b), Fe_3O_4/MOF/L-cysteine (c and d), and Fe_3O_4/MOF/L-cysteine after adsorption (e and f). EDS of Fe_3O_4/MOF/L-cysteine (g).
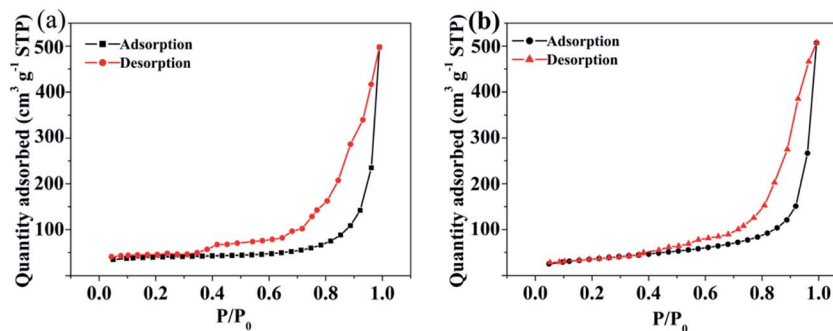
Fig. 4 N_2 adsorption–desorption isotherms of Fe_3O_4/MOF (a) and Fe_3O_4/MOF/L-cysteine (b).
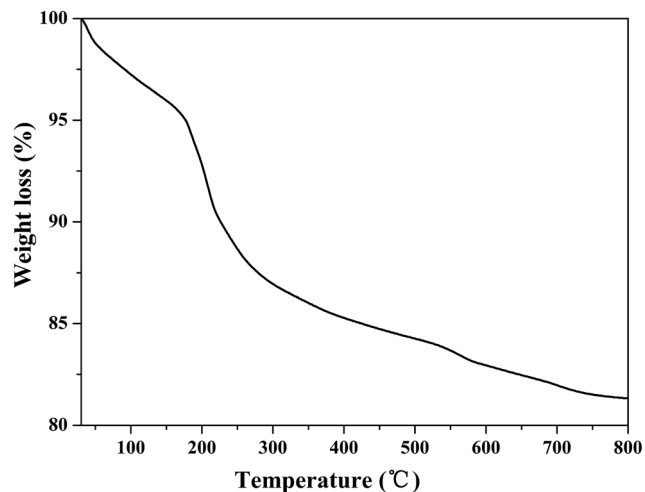
Fig. 5 TGA pattern of Fe_3O_4/MOF/L-cysteine.

Fig. 7 Cd(II) removal efficiency of different absorbents.

surface becomes closer, and the reason for this is the aggregation of L-cysteine on the loose surface of Fe_3O_4/MOF. The images of Fe_3O_4/MOF/L-cysteine after adsorption are shown in Fig. 3(e and f). It is clear that the surface morphology of Fe_3O_4/MOF/L-cysteine after adsorption stays the same as that of Fe_3O_4/MOF/L-cysteine before adsorption. This further proves the stability of Fe_3O_4/MOF/L-cysteine. In addition, the EDS of Fe_3O_4/MOF/L-cysteine is shown in Fig. 3(g). Cd is present in Fe_3O_4/MOF/L-cysteine, indicating successful adsorption of Cd(II).

Fig. 4 shows the N_2 adsorption–desorption isotherms of Fe_3O_4/MOF and Fe_3O_4/MOF/L-cysteine. Fe_3O_4/MOF and Fe_3O_4/MOF/L-cysteine have typical type IV curves with hysteresis loops, which are characteristic of mesoporous materials. The BET surface areas of Fe_3O_4/MOF and Fe_3O_4/MOF/L-cysteine are determined to be 666.18 $m^2 g^{-1}$ and 413.67 $m^2 g^{-1}$. The average pore sizes of Fe_3O_4/MOF and Fe_3O_4/MOF/L-cysteine are determined to be 23.16 nm and 16.45 nm. It is clear that the surface area, pore volume and pore size are all decreased after L-cysteine
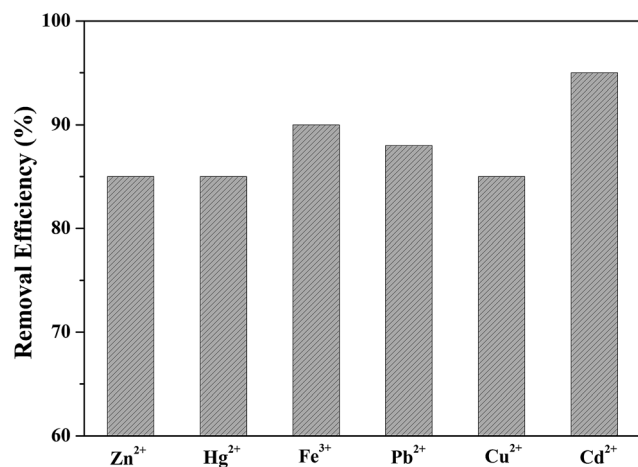
is added. This can be explained by the fact that the L-cysteine fills the pores to form a new composite.

The thermal stability of Fe_3O_4/MOF/L-cysteine was investigated using TGA, as shown in Fig. 5. The 5% mass loss from the beginning to 180 °C results from the loss of adsorbed water from the composite. A mass loss of about 8% can be seen from 180 °C to 300 °C, which can be explained by the decomposition of the L-cysteine over 180 °C. The mass loss of approximately 7% is mainly because of the collapse of the MOF skeleton. These results further prove the composition of the composite.

3.2. The adsorption properties

3.2.1 The adsorption of different heavy metal ions. The adsorption of different heavy metal ions is discussed, and the result is shown in Fig. 6. It is observed that Fe_3O_4/MOF/L-cysteine has the potential for the adsorption of a series of heavy metal ions, such as Cd(II), Zn(II), Fe(III), Cu(II), Hg(II), and Pb(II). The lowest removal efficiency of Fe_3O_4/MOF/L-cysteine is still over 80%. Even though the selectivity for different metal ions
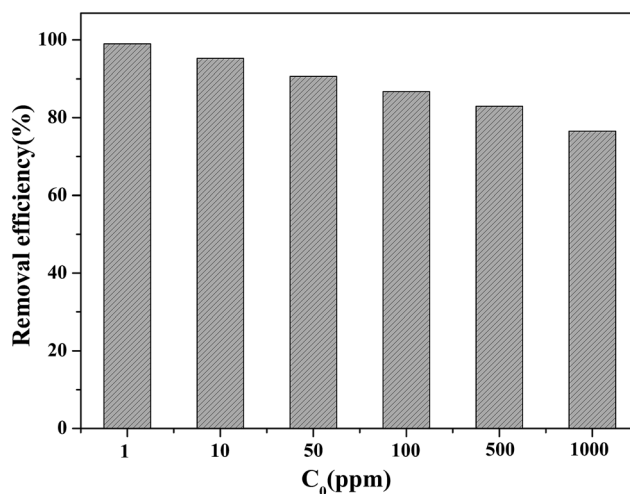

Fig. 6 The adsorption of different heavy metal ions.

Fig. 8 Effect of different concentrations of Cd(II) on adsorption.

Table 1 The maximum adsorption capacity for Cd(II)

Absorbent	Q_{max} (mg g^{-1})	Ref.
P (AANa-co-AM) GO	196.4	20
GOM	91.01	21
SiO$_2$/TiO$_2$	107.17	22
Cotton-PSMP-TMPyP	97.06	23
Fe$_3$O$_4$/MOF/L-cysteine	248.24	This work

was not clear, Fe$_3$O$_4$/MOF/L-cysteine has excellent adsorption properties for heavy metal ions. The removal efficiency for Cd(II) is the best, and the removal efficiencies of different metal ions were a little different, the reason for which is probably the different coordination forces between different heavy metal ions and the functional group of –SH in L-cysteine. In addition, the sizes of the different metal ions will have an effect on the physical adsorption of the porous MOFs.

3.2.2 Effect of different absorbents. The adsorption for Cd(II) of different adsorbents is compared, as shown in Fig. 7. It shows that the Cd(II) removal efficiencies of L-cysteine, Fe$_3$O$_4$/MOF and Fe$_3$O$_4$/MOF/L-cysteine are about 58%, 62% and 98%, respectively. It is obvious that the removal efficiency of Fe$_3$O$_4$/MOF/L-cysteine is much higher than that of L-cysteine and Fe$_3$O$_4$/MOF, the possible reason for which is that Fe$_3$O$_4$/MOF/L-cysteine demonstrates both physical adsorption by the MOF and chemical coordination between –SH in L-cysteine with Cd(II). Therefore, Fe$_3$O$_4$/MOF/L-cysteine is chosen to be the optimal absorbent for the next experiments.

3.2.3 Effect of different concentrations of Cd(II). The effect of the Cd(II) concentration on Cd(II) removal is discussed, and the result is shown in Fig. 8. It is clear that the Cd(II) removal efficiency is as high as 97% at low concentration. When the Cd(II) concentration increases to 1000 ppm, the removal efficiency can still be over 75%. This indicates that Fe$_3$O$_4$/MOF/L-cysteine has excellent adsorption not only at low concentrations but also at high concentration. When the concentration of Cd(II) is in a lower range (1–100 ppm), the removal efficiency is higher than 90%, while at higher concentrations, the removal efficiency decreases a little, but still stays above 80%. The reason is that the adsorption equilibrium constant is the same when the temperature remains unchanged. When the Cd(II) content increases, the adsorption rate becomes fast, so the adsorption reaches

equilibrium sooner, which will result in the decrease of the ratio of the adsorbed Cd(II) to the total amount of Cd(II). In this work, the concentration of 1.000 ppm Cd(II) is chosen and the maximum adsorption capacity is calculated to be 248.24 mg g^{-1}.

The maximum adsorption capacities of different adsorbents are shown in Table 1. This shows that the maximum adsorption capacity of Fe$_3$O$_4$/MOF/L-cysteine is greater than that of other recently reported adsorbents.

3.2.4 The adsorption mechanics. The time-dependent adsorption capacity is determined to investigate the kinetics of the adsorption of Cd(II) on Fe$_3$O$_4$/MOF/L-cysteine. The adsorption models are usually used to understand the mechanism of metal adsorption and the performance of the adsorbents for metal removal. The pseudo-first-order kinetic and pseudo-second-order kinetic model are the most typical ones. The pseudo-first-order model is expressed in the following way:

$$\ln(q_e - q_t) = \ln q_e - k_1 t \quad (1)$$

where k_1 (min^{-1}) is the pseudo-first-order rate constant, and q_e (mg g^{-1}) and q_t (mg g^{-1}) are the extents of adsorption at equilibrium and at time t, respectively. Therefore, the rate equation is obeyed when a linear relationship exists between $\ln(q_e - q_t)$ and t, in which case k_1 may be estimated from the gradient of the plot.

The pseudo-second-order model is expressed as:

$$\frac{t}{q_t} = \frac{1}{k_2 q_e^2} + \frac{t}{q_e} \quad (2)$$

where k_2 (g mg^{-1} min^{-1}), the gradient of a linear plot of t/q_t against t, is the pseudo-second-order rate constant.

The application of the pseudo-first-order and pseudo-second-order kinetic models to the adsorption of Cd(II) onto Fe$_3$O$_4$/MOF/L-cysteine has been investigated and the results are shown in Fig. 9. It is found that the regression coefficient of R^2 for the pseudo-second-order model ($R^2 = 0.9998$) is higher than that for pseudo-first-order. Hence, the pseudo-second-order kinetic model affords a more appropriate description of the adsorption process of Cd(II) on Fe$_3$O$_4$/MOF/L-cysteine.

To describe the adsorption isotherm and analyze the equilibrium data more scientifically, the Langmuir adsorption isotherm and Freundlich adsorption isotherm are employed. The Langmuir isotherm is expressed as:
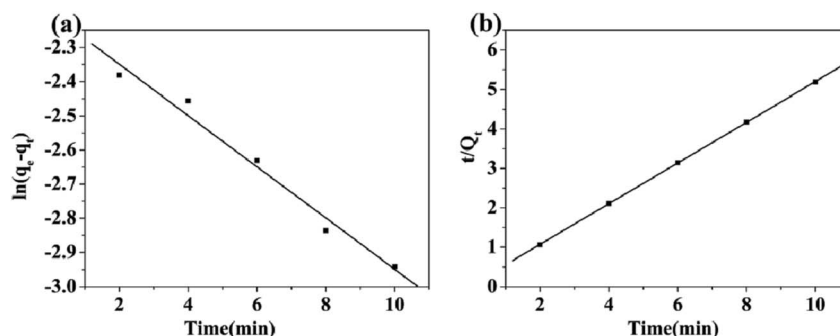

Fig. 9 Pseudo-first-order kinetic plot (a) and pseudo-second-order kinetic plot (b) for the adsorption of Cd(II) on Fe$_3$O$_4$/MOF/L-cysteine.
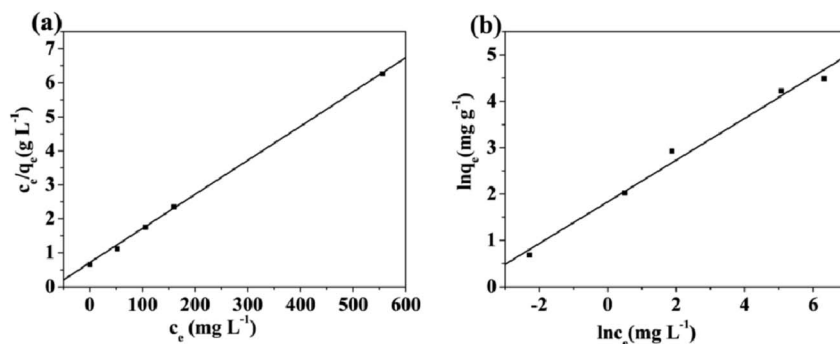
Fig. 10 Adsorption isotherms fitted by the Langmuir (a) and Freundlich (b) models for Cd(II) on Fe_3O_4/MOF/L-cysteine.

Table 2 Thermodynamic equilibrium constant K and relative thermodynamic parameters

T (K)	K	ΔH (kJ mol^{-1})	ΔS (J mol^{-1} K^{-1})	ΔG (kJ mol^{-1})
295	64.56			−10.22
305	120.87	−44.16	184.5	−12.16
315	206.67			−13.96

$$\frac{c_e}{q_e} = \frac{1}{q_{max}}K_L + \frac{c_e}{q_{max}} \quad (3)$$

where c_e (mg L^{-1}) is the equilibrium concentration of Cd(II), q_e (mg g^{-1}) is the equilibrium adsorption capacity, q_{max} (mg g^{-1}) is the maximum adsorption capacity in the calculation, and K_L (L mg^{-1}) is the Langmuir adsorption constant, related to the free energy of adsorption. A linear relationship exists between c_e/q_e and c_e, which is obtained from the Langmuir model, as shown in Fig. 10(a).

The Freundlich isotherm is expressed as:

$$\ln q_e = \ln K_F + \frac{1}{n}\ln c_e \quad (4)$$

where K_F (mg g^{-1}) and $1/n$ are the Freundlich adsorption constants corresponding to adsorption capacity and adsorption intensity, respectively; c_e (mg L^{-1}) is the equilibrium concentration of Cd(II), and q_e (mg g^{-1}) is the equilibrium adsorption capacity. The gradient of a linear plot of $\ln q_e$ against $\ln c_e$ is

obtained from the Freundlich model as shown in Fig. 10(b). It is found that the value of R^2 for the Langmuir model ($R^2 = 0.9998$) is higher than that for the Freundlich model ($R^2 = 0.9684$), indicating that the Langmuir adsorption model is more suitable for describing the adsorption isotherm of Cd(II) on the absorbent. This implies that the surface of the material is more homogeneous, with a predominant chemical adsorption mechanism.

In the process of the adsorption of Cd(II), the thermodynamic equilibrium constant (K) and the free energy change (ΔG) were determined by changing the experimental temperatures to be 295 K, 305 K and 315 K. The energy change of adsorption is calculated using the following equations:

$$K = q_e/c_e \quad (5)$$

$$\Delta G = -RT \ln K \quad (6)$$

where R is the thermodynamic constant and T is the experimental temperature. If the enthalpy change (ΔH) does not vary significantly with the temperature change, its value and that of entropy change (ΔS) can be calculated from the van't Hoff equation:

$$\ln K = -\frac{\Delta H}{RT} + \frac{\Delta S}{R} \quad (7)$$

where K, ΔH, ΔS, and ΔG are obtained from the above equations. The results are shown in Table 2. The free energy (ΔG) is negative, indicating that the adsorption of Cd(II) is spontaneous. The positive enthalpy change (ΔH) means that the
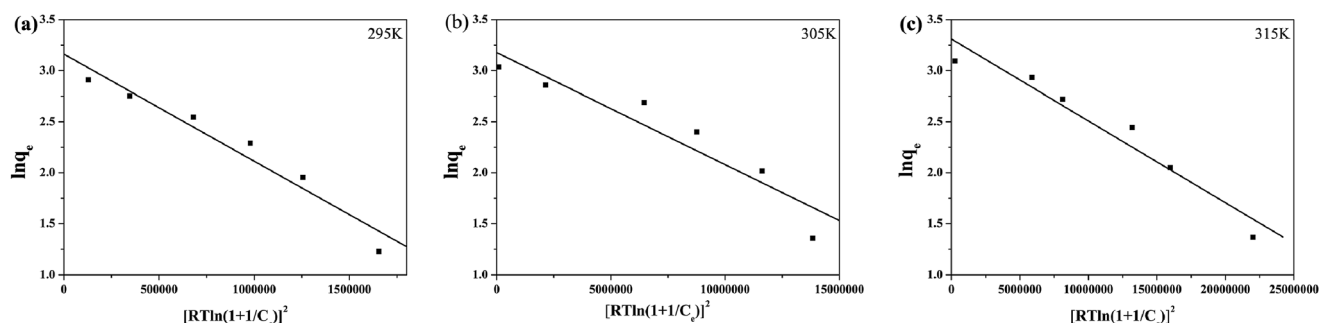

Fig. 11 Dubinin−Radushkevich (D−R) isothermal adsorption model of Fe_3O_4/MOF/L-cysteine for removal of Cd(II) at 295 K (a), 305 K (b), and 315 K (c).
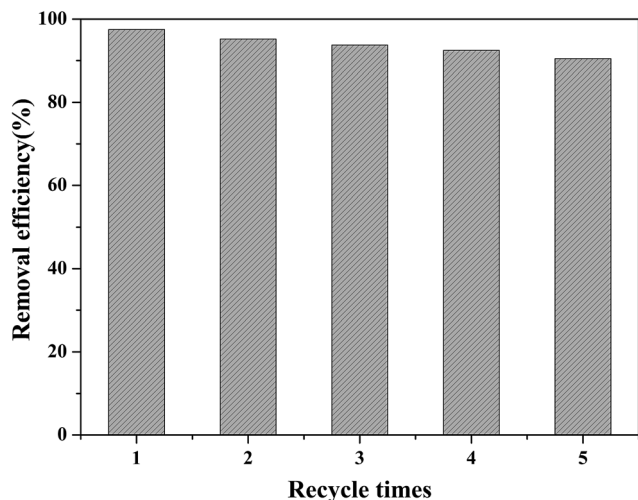
Fig. 12   Effect of the number of recycling times of the absorbent.

process is an endothermic process. Hence, the higher the temperature, the better the removal efficiency.

3.2.5   Dubinin–Radushkevich (D–R) isotherm. The Dubinin–Radushkevich (D–R) isotherm adsorption process was then investigated to understand the principle of adsorption, *i.e.*, chemical adsorption and/or physical adsorption processes.[24] The Dubinin–Radushkevich (D–R) isothermal adsorption model can be described as:

$$\ln Q_e = \ln Q_m - B_d [RT \ln(1 + 1/c_e)]^2 \tag{8}$$

$$E = 1/(2B_d)^{1/2} \tag{9}$$

where Q_e is the equilibrium adsorption capacity of Cd(II) on Fe$_3$O$_4$/MOF/L-cysteine (mg g^{-1}), B_d (mol^2 J^{-2}) is the activity factor correlated with the mean free energy of adsorption, R is the ideal gas constant (8.314 J mol^{-1} K^{-1}), T (K) is the Kelvin temperature, and E (kJ mol^{-1}) is the average free energy of adsorption. Chemical adsorption normally showed the energy E

in the range of 8–16 kJ mol^{-1}, while physical adsorption happened when E was less than 8.

Linear plots between $\ln Q_e$ and $RT \ln(1 + 1/c_e)^2$ at different temperatures are shown in Fig. 11. The D–R constants were estimated using the intercepts and slopes of linear plots. For the adsorption process for Cd(II), E was calculated to be 2.49, 5.13 and 8.91 kJ mol^{-1} at different temperatures (a, b and c), respectively. It can be concluded that the driving force was mainly physical adsorption at low temperature. With increasing temperature, the main driving force was chemical adsorption resulting from the coordination between Cd(II) and L-cysteine. The conclusion is consistent with the FT-IR spectrum of Fe$_3$O$_4$/MOF/L-cysteine after adsorption.

3.2.6   Regeneration of Fe$_3$O$_4$/MOF/L-cysteine. To evaluate the possibility of regeneration and reusability of Fe$_3$O$_4$/MOF/L-cysteine as an adsorbent, desorption experiments were performed. 1.0 mol L^{-1} HCl solution was used to regenerate the absorbent. The effect of five consecutive adsorption–desorption cycles were studied, and the results are shown in Fig. 12. It is obvious that the removal efficiency of Cd(II) on Fe$_3$O$_4$/MOF/L-cysteine decreases slightly with increasing cycle number. The Cd(II) removal efficiency almost maintains a steady value and it is still above 90% after 5 times of recycling. This indicates that Fe$_3$O$_4$/MOF/L-cysteine has excellent reusability for magnetic solid phase extraction to determine trace amounts of Cd(II).

3.3.   Optimization of MSPE procedure

Because of the excellent adsorption properties of Fe$_3$O$_4$/MOF/L-cysteine, the MSPE procedure was set up and the extraction was optimized.

3.3.1   Effect of the amount of Fe$_3$O$_4$/MOF/L-cysteine. The effect of the amount of Fe$_3$O$_4$/MOF/L-cysteine on the extraction was investigated. The removal efficiency increases with an increased amount of Fe$_3$O$_4$/MOF/L-cysteine, as shown in Fig. 13. When the amount of Fe$_3$O$_4$/MOF/L-cysteine exceeds 50 mg, the removal efficiency changes slightly. To ensure that there is
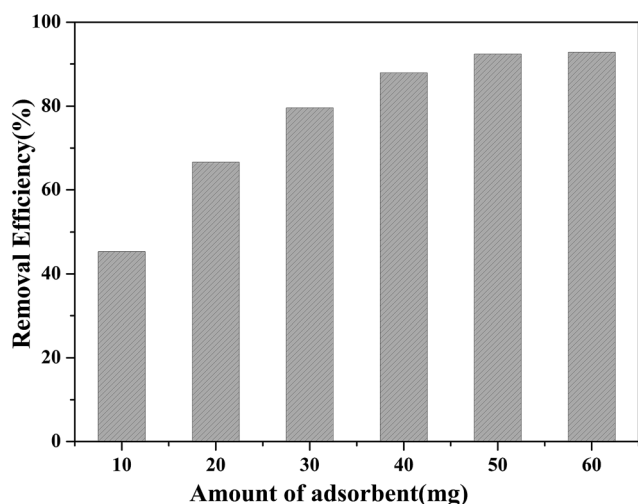

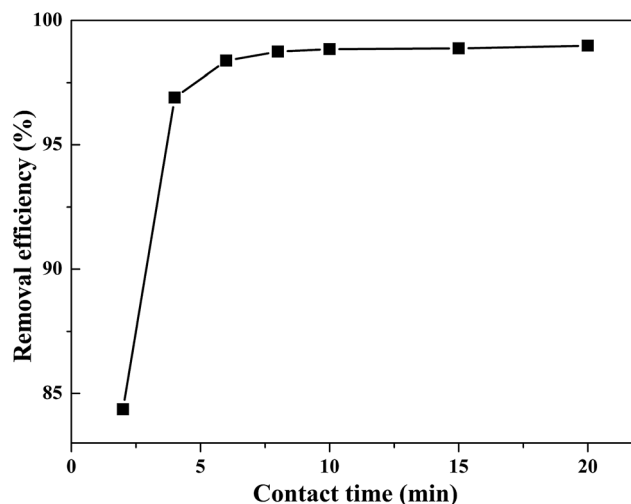Fig. 13   Effect of the amount of Fe$_3$O$_4$/MOF/L-cysteine on adsorption.

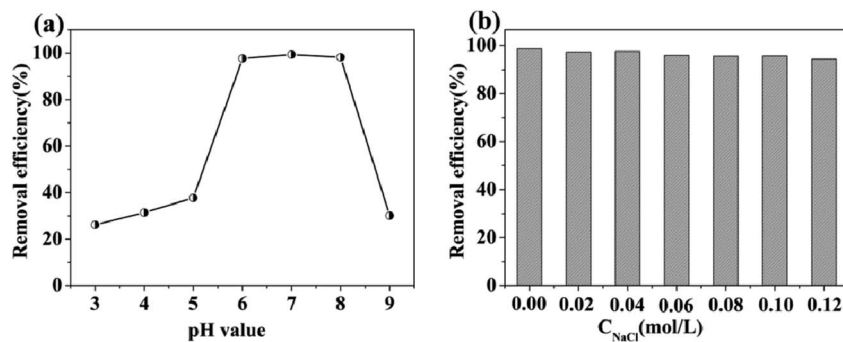Fig. 14   Effect of contact time on adsorption.

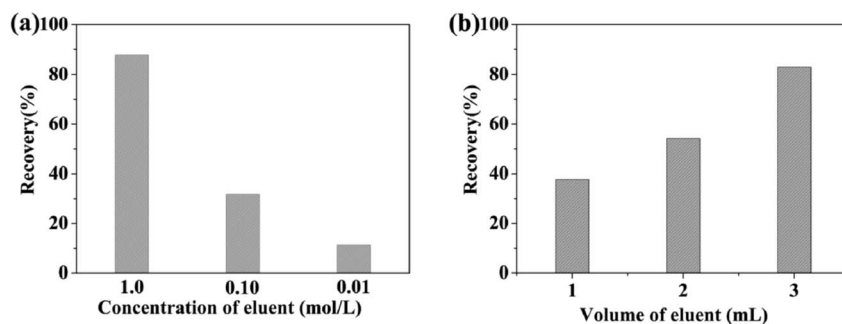Fig. 15   Effect of pH (a) and effect of ionic strength (b).

Fig. 16   Effect of the concentration of the eluent (a) and effect of the volume of the eluent (b).

enough adsorbent for the extraction, 50.00 mg of Fe_3O_4/MOF/L-cysteine was chosen for the following experiments.

3.3.2   Effect of extraction time. Fig. 14 shows the effect of contact time on Cd(II) removal. The results indicate that the reaction reaches adsorption equilibrium very fast, and the removal efficiency of Cd(II) increases slightly from 10 min to 20 min. Therefore, to ensure that the extraction time is sufficient for adsorption, 10 min is chosen as the contact time.

3.3.3   Effect of pH and ionic strength. Fig. 15(a) shows the effect of pH value on the extraction. It shows that the removal efficiency of Cd(II) at pH 9.0 and pH 3–5 are very low. The effect at pH 9.0 can be explained by the fact that the Cd(II) ions are separated out as a $Cd(OH)_2$ precipitate. As for the low removal efficiency at pH 3–5, a possible reason is that the adsorbed Cd(II) is eluted out from Fe_3O_4/MOF/L-cysteine because of the destruction of the coordination bond between the Cd(II) and the functional groups of L-cysteine. The removal efficiency of

Cd(II) is up to 97% in the pH range of 6.0 to 8.0. In such cases, Fe_3O_4/MOF/L-cysteine can be used to remove heavy metal ions. Therefore, pH 7.0 is selected in the experiments. The effect of ionic strength was investigated by changing the NaCl concentrations from 0 mol L^{-1} to 0.12 mol L^{-1} and the results are shown in Fig. 15(b). It is clear that the removal efficiency for Cd(II) hardly changes with increased NaCl concentration, which indicates that the system is scarcely affected by ionic strength.

Table 3   Tests of addition/recovery in the experiments for Cd(II), $N = 5^a$

Sample	Amount of Cd(II) (ng)		Recovery(%)
	Added	Found	
Tap water	—	ND	98.7%
	1.0	0.987	
Lake water	—	ND	105.4%
	1.0	1.054	

[a] ND: not found. The volume of the solution is 100 mL.
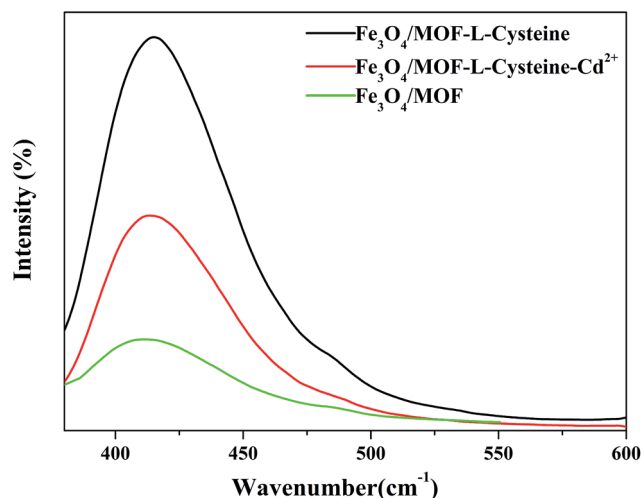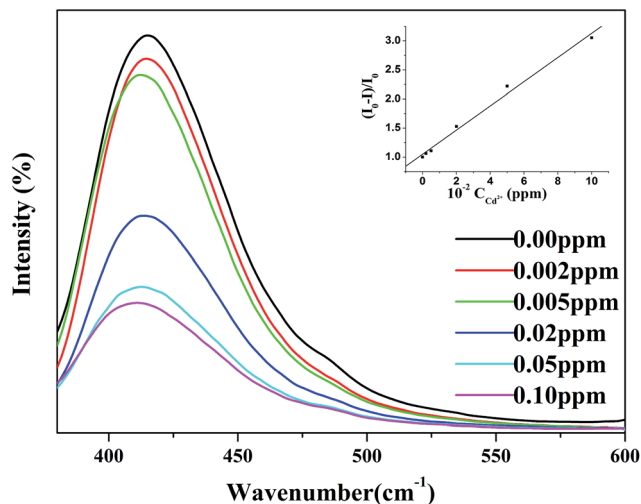

Fig. 17   Effect on luminescence intensity of absorbent.

Fig. 18 Fluorescence emission spectra of the Fe$_3$O$_4$/MOF/L-cysteine sensor exposed to various concentrations of Cd(II): 0, 0.002, 0.005, 0.02, 0.05, and 0.1 ppm from top to bottom. The inset is the linear plot of the fluorescence intensity *versus* the concentration of Cd(II).

3.3.4 Desorption conditions. Different concentrations of hydrochloric acid solutions as the eluent are investigated and the results are shown in Fig. 16(a). It is obvious that 1.0 mol L^{-1} HCl is the most optimal eluent for desorption. Meanwhile, the effect of eluent volume was studied, as shown in Fig. 16(b). This shows that the recovery of Cd(II) increases with increased eluent volume, but increased elution volume will result in a decline in the analytical signal due to the dilution effect. Therefore, 1 mL 1.0 mol L^{-1} HCl is chosen for the eluent in the extraction.

The absorbent Fe$_3$O$_4$/MOF/L-cysteine was applied in MSPE to determine and enrich trace amounts of Cd(II) using ICP-AES spectra. The results show that the preconcentration factor is 94, and the determination limit is 10.6 ng mL^{-1}.

3.3.5 Sample analysis. The developed method based on Fe$_3$O$_4$/MOF/L-cysteine was evaluated for its potential application in Cd(II) extraction from tap water and lake water, and the results are shown in Table 3. It can be seen that Cd(II) is not

found in tap water or lake water. The recovery values for Cd(II) are in the range of 98.7–105.4%.

3.4. Fluorescence sensing of Cd(II)

To examine the potential as a sensor for Cd(II) of Fe$_3$O$_4$/MOF/L-cysteine, the fluorescence properties of Fe$_3$O$_4$/MOF/L-cysteine are discussed, as shown in Fig. 17. It can be seen that the fluorescence intensity of Fe$_3$O$_4$/MOF at 415 nm is weak. After formation of the composite Fe$_3$O$_4$/MOF/L-cysteine, the intensity increases a lot. When 0.02 ppm Cd(II) is added into Fe$_3$O$_4$/MOF/L-cysteine, the intensity decreases clearly. It is obvious that Fe$_3$O$_4$/MOF/L-cysteine can potentially be used as a fluorescent probe for "turn-off" detection of Cd(II).

The relationship between the fluorescence intensity and Cd(II) concentration was investigated, as shown in Fig. 18. It was found that the fluorescence of Fe$_3$O$_4$/MOF/L-cysteine becomes more quenched with increased Cd(II) concentration. When the Cd(II) concentration is in the range of 0.00 to 0.100 ppm, there is a linear relationship between decreased intensity and Cd(II) concentration. The good linear correlation is shown as the following equation:

$$(I_0 - I)/I_0 = 208.01[C] + 1.0487 \qquad (10)$$

where I_0 and I express the fluorescence intensities of Fe$_3$O$_4$/MOF/L-cysteine at 415 nm in the absence and presence of Cd(II) respectively, and [C] is the Cd(II) concentration. The LOD is 0.93 ng mL^{-1}. The relative standard deviation (RSD) was calculated to be 4.68%.

3.5. Comparison with other materials

A comparison with recently reported materials for the removal of Cd(II) is shown in Table 4. It can be concluded that Fe$_3$O$_4$/MOF/L-cysteine is suitable for application in magnetic solid phase extraction and fluorescence sensing of Cd(II).

4. Conclusion

In this work, Fe$_3$O$_4$/MOF/L-cysteine is successfully synthesized and applied for the removal of Cd(II) from wastewater. Compared to Fe$_3$O$_4$/MOF and L-cysteine, Fe$_3$O$_4$/MOF/L-cysteine shows better removal efficiency for Cd(II), indicating that L-cysteine plays an important role in increasing the adsorption capacity of Cd(II) in solution. The kinetics for the adsorption and the adsorption isotherms were investigated and the results indicate that the pseudo-second-order kinetics model matches with the adsorption of Cd(II) on Fe$_3$O$_4$/MOF/L-cysteine. The Langmuir model is more suitable for describing the adsorption behavior on Fe$_3$O$_4$/MOF/L-cysteine.

The desorption experiment indicates that Fe$_3$O$_4$/MOF/L-cysteine has great prospects in the removal of heavy metal ions in the area of industrial wastewater treatment. Furthermore, the absorbent Fe$_3$O$_4$/MOF/L-cysteine was applied in MSPE to determine and enrich the trace amount of Cd(II) using ICP-AES spectroscopy. The results show that the determination limit is 10.6 ng mL^{-1} and the recovery values for Cd(II) are in the range

Table 4 Comparison with previously reported methods of the detection limit of Cd(II)

Material	Method	LOD (μg L^{-1})	Ref.
Eu^{3+}/Uio-66(Zr)–(COOH)$_2$	Fluorescent sensor	6.74	25
Fe$_3$O$_4$/ZrO$_2$	ICP-AES	1.01	26
Fe$_3$O$_4$-ethylenediamine/MIL-101(Fe)	FAAS	1.05	27
Cd^{2+}-selective electrode	Electrochemical sensor	1.45	28
Rhodamine derivative	Fluorescent sensor	1.15	29
Fe$_3$O$_4$/MOF/L-cysteine	Fluorescent sensor	0.94	This work
Fe$_3$O$_4$/MOF/L-cysteine	ICP-AES	10.60	This work

of 98.7–105.4%. Furthermore, Fe_3O_4/MOF/L-cysteine can also be a fluorescent sensor for detecting ultra low concentrations of Cd(II), and the detection limit (LOD) and relative standard deviation (RSD) were calculated to be 0.94 ng mL^{-1} and 6.48%, respectively. Thus, it can be seen that Fe_3O_4/MOF/L-cysteine not only is an excellent absorbent to detect trace amounts of Cd(II) by ICP-AES spectroscopy, but also as a fluorescent sensor detects ultra low concentrations of Cd(II) by fluorescence spectroscopy.

Conflicts of interest

There are no conflicts to declare.

Acknowledgements

References

1 A. Rani, A. Kumar, A. Lal and M. Pant, *Int. J. Environ. Health Res.*, 2014, **24**, 378.

2 Y. Chen, Z. P. Chen, S. Y. Long and R. Yu, *Anal. Chem.*, 2014, **86**, 12236.

3 M. Asgher, M. Khan, N. Anjum and N. K. Han, *Protoplasma*, 2015, **252**, 399.

4 K. F. Lam, K. L. Yeung and G. Mckay, *Environ. Sci. Technol.*, 2007, **41**, 3329.

5 R. B. Priscilla, M. B. Carla, P. Verónica, P. Jorge, A. H. Juan, R. P. Catalina and A. M. Ana, *Talanta*, 2015, **139**, 13.

6 Y. Gao, S. D. Galan, A. D. Brauwere, W. Baeyens and M. Leermakers, *Talanta*, 2010, **82**, 1919.

7 S. H. Huo and X. P. Yan, *Analyst*, 2012, **137**, 3445.

8 J. Zhang, J. Han, M. Wang and R. Guo, *J. Mater. Chem. A*, 2017, **5**, 4058.

9 S. Lin, Y. Yang, G. Chen, X. Chen, W. Zhang and M. Xu, *Appl. Surf. Sci.*, 2017, **425**, 141.

10 D. Chen, T. Awut, B. Liu, Y. Ma, T. Wang and I. Nurulla, *E-Polymers*, 2016, **16**, 313.

11 M. Safari, Y. Yamini and M. Y. Masoomi, *Mikrochim. Acta*, 2017, **184**, 1555.

12 W. Yang, H. Chen and T. Jie, *Food Chem.*, 2015, **181**, 191.

13 K. Xing, R. Fan, J. Wang, S. Zhang, K. Feng, X. Du, Y. Song, P. Wang and Y. Yang, *ACS Appl. Mater. Interfaces*, 2017, **9**, 1988.

14 J. Li, B. Wu, Q. Zhang, H. Wang and Y. Li, *J. Nanosci. Nanotechnol.*, 2016, **16**, 9568.

15 W. Wu, B. Li, C. Gu, J. Wang, A. Singh and A. Kumar, *J. Mol. Struct.*, 2017, **1148**, 531.

16 J. Liu, Z. Sun, Y. Deng, Y. Zou, C. Li, X. Guo, L. Xiong, Y. Gao, F. Li and D. Zhao, *Angew. Chem.*, 2009, **121**, 5989.

17 L. Li, K. K. Sun, L. Fan, W. Hong, Z. S. Xu and L. Liu, *Mater. Lett.*, 2014, **126**, 197.

18 Q. X. Liao, Z. J. Li, J. Zhang, Y. Kang and Y. M. Yao, *Acta Crystallogr., Sect. C: Cryst. Struct. Commun.*, 2004, **60**, m509.

19 C. D. Wu, C. Z. Lu, W. B. Yang, H. H. Zhuang and J. S. Huang, *Inorg. Chem.*, 2002, **41**, 3302.

20 J. Ma, K. Jia, G. Cheng and S. Zhang, *J. Environ. Eng.*, 2016, **142**, 04016062.

21 S. He, F. Zhang, S. Cheng and W. Wang, *ACS Sustainable Chem. Eng.*, 2016, **4**, 3948.

22 P. Tan, Y. Hu and Q. Bi, *Colloids Surf., A*, 2016, **509**, 56.

23 M. Waseem, S. T. Muntha, M. Nawaz, W. Rehman, M. A. Rehman and K. H. Shah, *Mater. Res. Express*, 2017, **4**, 1.

24 K. K. H. Choy, G. Mckay and J. F. Porter, *Resour., Conserv. Recycl.*, 1999, **27**, 1–2.

25 J. Hao and B. Yan, *Chem. Commun.*, 2015, **51**, 7737.

26 S. Zhu, F. Hu, D. Pan, W. Xu and N. Gan, *Adv. Mater. Res.*, 2012, **487**, 658.

27 M. Babazadeh, R. H. Khanmiri, J. Abolhasani, E. Ghorbani-Kalhor and A. Hassanpour, *RSC Adv.*, 2015, **2**, 32.

28 S. Yu, F. Li and W. Qin, *Sens. Actuators, B*, 2011, **155**, 919.

29 M. Maniyazagan, R. Mariadasse, J. Jeyakanthan, N. K. Lokanath, S. Naveen, K. Premkumar, P. Muthuraja, P. Manisankar and T. Stalin, *Sens. Actuators, B*, 2017, **238**, 565.